Materials Science and Engineering C 45 (2014) 698–708

Contents lists available at ScienceDirect

Materials Science and Engineering C

journal homepage: www.elsevier.com/locate/msec

Melt electrospinning of poly(ε-caprolactone) scaffolds: Phenomenological observations associated with collection and direct writing

Toby D. Brown [a], Fredrik Edin [a], Nicola Detta [a], Anthony D. Skelton [a], Dietmar W. Hutmacher [a,b,c,*], Paul D. Dalton [a,d,**]

[a] Institute for Health and Biomedical Innovation, Queensland University of Technology, 60 Musk Avenue, Kelvin Grove 4059, Australia
[b] Institute for Advanced Study, Technical University Munich, Lichtenbergstraße 2a, 85748 Garching, Germany
[c] George W Woodruff School of Mechanical Engineering, Georgia Institute of Technology, 801 Ferst Drive Northwest, Atlanta, GA 30332, USA
[d] Department of Functional Materials in Medicine and Dentistry, University of Würzburg, Pleicherwall 2, 97070 Würzburg, Germany

ARTICLE INFO

Article history:
Received 10 March 2014
Accepted 8 July 2014
Available online 15 July 2014

Keywords:
Electrospinning
Fibers
Tissue engineering
3D printing
Additive manufacturing
Electrohydrodynamic writing

ABSTRACT

Melt electrospinning and its additive manufacturing analogue, melt electrospinning writing (MEW), are two processes which can produce porous materials for applications where solvent toxicity and accumulation in solution electrospinning are problematic. This study explores the melt electrospinning of poly(ε-caprolactone) (PCL) scaffolds, specifically for applications in tissue engineering. The research described here aims to inform researchers interested in melt electrospinning about technical aspects of the process. This includes rapid fiber characterization using glass microscope slides, allowing influential processing parameters on fiber morphology to be assessed, as well as observed fiber collection phenomena on different collector substrates. The distribution and alignment of melt electrospun PCL fibers can be controlled to a certain degree using patterned collectors to create large numbers of scaffolds with shaped macroporous architectures. However, the buildup of residual charge in the collected fibers limits the achievable thickness of the porous template through such scaffolds. One challenge identified for MEW is the ability to control charge buildup so that fibers can be placed accurately in close proximity, and in many centimeter heights. The scale and size of scaffolds produced using MEW, however, indicate that this emerging process will fill a technological niche in biofabrication.

1. Introduction

One key area of tissue engineering (TE) research is the fabrication of scaffolds to provide a three-dimensional (3D) biocompatible support for cell migration, proliferation and differentiation [1]. In addition to being made from compatible materials with surface properties optimized for cell interactions, scaffolds require an interconnecting pore network to be cell-invasive. Ideally, the fabrication process should allow the scaffold design to be altered systematically so that an optimum scaffold architecture for each cell/tissue type can be established. There are numerous routes to scaffold fabrication, each with advantages and disadvantages in their processing and cellular response [2].

Melt electrospinning has recently emerged as a direct writing approach to the production of orderly porous structures for application in TE [3,4]. However, the ability to construct a machine which produces a high quality melt electrospun scaffold is more complex than for solution electrospinning, which comprises over 99.5% of the total electrospinning literature [5]. While the number of melt electrospinning publications is increasing, a lack of established research is part of the challenge with applying this technique to biofabrication. The low number of publications is due not only to the complexity of building a melt electrospinning machine for the laboratory, but also due to the micron-diameter fibers often attained: electrospinning is a field that has been focused towards nanotechnology [6,7]. Although melt electrospinning produces fibers from as low as 270 nm [8] to as large as 350 μm [9] in diameter, our experience finds that 5 to 25 μm is a more typical range. However, recent interest in TE scaffold fabrication using additive manufacturing (AM) approaches based on melt extrusion direct writing has added impetus to developing melt electrospinning as a direct writing process.

One key requirement in scaffold-based TE is a suitable scaffold pore size which promotes cell invasion and, in many instances, vascularization

* Correspondence to: D.W. Hutmacher, Institute for Health and Biomedical Innovation, Queensland University of Technology, 60 Musk Avenue, Kelvin Grove 4059, Australia.
** Correspondence to: P.D. Dalton, Department of Functional Materials in Medicine and Dentistry, University of Würzburg, Pleicherwall 2, 97070 Würzburg, Germany.
E-mail addresses: dietmar.hutmacher@qut.edu.au (D.W. Hutmacher), daltonlab@gmail.com (P.D. Dalton).

http://dx.doi.org/10.1016/j.msec.2014.07.034
0928-4931/

[10]. In the field of solution electrospinning, submicron diameter fibers provide high specific areas for cell attachment [11,12]. However, fibers collected onto a flat stationary substrate deposit randomly to create a tightly packed nonwoven mesh with pore sizes too small for cell penetration [13,14]. Therefore, collector modifications are required in order to generate scaffolds with pore sizes large enough to promote cell infiltration in to the scaffold [1,15–18], where the charged fibers make it challenging to control fiber placement to create ordered structures and limit the achievable thickness. The accumulation and removal of toxic solvents present further challenges, particularly for medical purposes [19,20].

Despite allowing polymers to be processed as received without the need for toxic solvents, 3D printing for TE based on melt extrusion direct writing faces different challenges to electrospinning: where the current gold standards can only achieve filament diameters several orders of magnitude larger than electrospinning [3,4]. On the other hand, direct melt writing techniques offer precise control over filament placement to create 3D structures with highly ordered pores, sufficiently large (above 100 μm) to encourage both cell infiltration and vascularization [10]. In some respects melt electrospinning is similar to melt extrusion, also avoiding the use of toxic solvents in solution electrospinning. Whereas in melt extrusion the filament resolution is limited by the nozzle size through which polymer can be extruded, the addition of high voltage (HV) to the nozzle in melt electrospinning causes the polymer to become charged and deform into an electrostatically drawn jet which reduces the filament diameter to magnitudes approaching solution electrospinning [5].

Collector modifications have recently been demonstrated to produce TE scaffolds with pore sizes sufficient for cell penetration [21–23], though the added requirement to provide pores above 100 μm for vascularization highlights the need for improvement over the control of melt electrospun fiber deposition. Compared to the unstable solution electrospinning jet, the melt electrospinning jet is relatively focused [8,24], making it appear more suitable to be adopted as a direct writing approach. Combining melt electrospinning with a translating collector to direct-write 3D structures was only recently reported [4,25], and is promising for the creation of ordered structures, with a total of eight papers from six different laboratories developing this approach published in the past three years [3,4,9,21,26–29]. However, viscoelastic melt electrospun fibers will coil under compression as they deposit and solidify onto a collector that is moving slower than the melt flow in the electrified molten jet [4].

This article aims to report observed phenomenological aspects of melt electrospun fiber deposition, including coiling of the melt jet and disturbing charge interactions. A variety of collection configurations are investigated, towards improving the ability to accurately place fibers. Dynamic collection methods such as melt electrospinning writing (MEW) are explored as a 3D printing approach to fabricate cell invasive scaffolds with interconnected pores large enough to be suitable for vascularization.

2. Materials & methods

2.1. Materials

All scaffolds were produced with a biodegradable polymer, poly(ε-caprolactone) (PCL), which has increasing utility within TE [30]. Two sources of PCL were melt electrospun in this paper: CAPA 6500C (Perstop Chemicals, UK); and one purchased from Sigma (Australia) (80,000 g/mol.). Table 1 presents the type of PCL used in each experiment. In each experiment PCL was used as received—prior to electrospinning, the pellets were placed directly into a 3 mL plastic syringe (B-Braun, Australia), capped with a female Luer-Lok block and heated to 90 °C with the syringe held upright. Once the PCL was molten, the cap was removed and the plunger was drawn back and forth in the syringe to purge air bubbles from the polymer melt. A blunt Luer-Lok needle (21 G/23 G, B-Braun, Australia) was then attached to the syringe.

2.2. Melt electrospinning device

A melt electrospinning apparatus was custom-made, consisting of: a Perspex enclosure; a thermoregulated water bath recirculating heated water through a glass jacket into which a plastic Luer-lock syringe containing the PCL was placed; a programmable syringe pump connected to the syringe plunger to feed the molten polymer at a desired flow rate through a blunt needle; and a HV supply, which was connected to the needle, to create an electric field across an air gap to a grounded collector.

Various collector substrates were used, including a stationary patterned electroconductive collector, an array of patterned hemispherical collectors; and smooth collector surfaces. As shown in Fig. 1, only the flat aluminum (Al) or Superfrost® yellow glass microscope slides (Lomb Scientific, Australia) were assessed as collector substrates for use in a direct writing method. A translating x–y stage from Velmex Inc. (USA) was assembled with a motor/driver kit supplied by Ocean Controls (Australia), and various collector substrates were placed on an electrically grounded moving platform to automate the fiber collection process. The x–y stage was placed below the spinneret and computer programs written in G-Code were used to control the movement of the x–y stage.

This study presents a diverse set of experiments, and as such the instrument parameters used in each experiment are described in Table 1. In general, the instrument parameters included: an applied voltage of 9–10 kV; a collection distance of 10–30 mm; a flow rate of 10–20 μL/h; and a melting temperature of 80–90 °C. For all experiments, the melt electrospinning jet was allowed to stabilize for at least 2 min before collection commenced.

2.3. Melt electrospinning onto patterned electroconductive collectors

Stainless steel shaving blades were used as flat collectors, with either circular or diamond shaped voids arranged in repeating patterns, to investigate the ability to create porous structures using a template approach. The diameter of each circular void was approximately 500 μm, while the long axis of the diamond-shaped voids was also approximately 500 μm. In each case, the voids in the collectors were spaced a minimum distance of approximately 150 μm. These collectors were placed on the grounded collector platform so that they too became grounded.

To upscale and automate this collection process, readily available tap filters (with a similar 400 μm × 400 μm square void template architecture) were placed in a 4 × 5 array onto the grounded moving collector. A computer program was written so that the first tap filter collector was located centrally under the spinneret. The program paused so that the melt electrospinning jet deposited for 20 min onto the tap filter, and then translated the grounded platform so that the second tap filter was located directly under the spinneret. The collection period of 20 min was repeated and the sequence continued until fibers were collected for 20 min on all 20 of the filters.

2.4. Electrospinning onto microscope slides

Glass microscope slides were placed directly on top of the electrically grounded moving platform to assess their feasibility as a fiber collection substrate compared to metallic surfaces. The microscope slides were also wrapped in Al foil and placed on the same grounded surface to act as a control. Fibers were collected for varying time periods to assess if the material differences caused variations in fiber collection over time. A computer program was written to control the movement of the grounded platform and hence automate this process (G-code provided in supplementary data).

Table 1
Summary of the instrument parameters for the different experiments performed.

Configuration	Polymer	Temperature (°C)	Voltage (kV)	Flow rate (μL/h)	Collector distance (mm)	Spinneret diameter (gauge)	Figure
Flat collector	Sigma	90	4, 6, 8, 10, 12	5, 10, 20	20, 30, 40, 60	21	2
Patterned collector	Sigma	90	10	50	40	21	3
Convex patterned collector	Sigma	90	8	10	70	21	4
Microscope slides—spots	Sigma	90	12	5	20, 50	21	5–7
MEW	CAPA 6500C	80	12	10, 20	20	23	8
MEW—stacking	Sigma	80	13	20	20	21	9
MEW—placement	Sigma	80	14	5–20	20	21	10

The collector translated 5 mm in the positive x-direction before pausing for a defined period. Following this pause, the collector would again translate 5 mm in the same direction before pausing for an increased time period. This sequence was repeated, where the dwell times were increased according to the following series: 1 s; 2 s; 5 s; 10 s; 20 s; 50 s; and 100 s. Following the 100 s pause period, the stage translated 5 mm perpendicular to the initial direction of movement (positive y-direction) and then dwelled for a period of 100 s. The collector then translated in the negative x-direction, repeating the pause sequence, this time in reverse order (decreasing increments in dwell time) towards the starting point ($x = 0$). Following another 5 mm positive y-direction translation ($y = 10$ mm), the process was repeated so that four samples for each collection time were located on the same microscope slide (28 samples per slide). The fiber diameter and average deposition area, along with the standard deviation, for each collection interval were measured on multiple slides ($n = 8$).

2.5. Melt electrospinning writing

A program was written to translate the collector platform following a square wave pattern. The translation speed was incrementally increased for each line to assess the effects on fiber deposition. Fiber diameters were measured for each translation speed using optical microscopy (OM) as described below. To assess the ability to stack fibers and create 3D structures using MEW, a second program continuously traced a square wave pattern, where upon completion of each circuit the pattern was rotated 90°. Box-like structures were generated with each fibrous layer orientated at 90° to the previous layer. A turning compensation component was incorporated into the program so that rapid changes of direction did not affect the fiber stacking experiment. A third program incrementally varied the distance between parallel lines in the square wave to assess fiber placement accuracy. Examples of the G-code programs are provided in the supplementary data.

2.6. Optical microscopy (OM) and scanning electron microscopy (SEM) characterization

When imaging using OM, scaffolds on microscope slides were visualized using an Imager A1 Axio optical microscope, equipped with a digital camera (Zeiss, Australia). High (40×) magnification pictures for fiber diameter measurement were acquired using AxioVision software. Prior to SEM imaging, scaffolds were mounted onto SEM stubs using carbon tape then gold sputter coated and imaged using an FEI Quanta 200 Environmental SEM operating at 10 kV. For diameter measurements two crossed, straight lines were arbitrarily drawn through an SEM image. The diameter of all the fibers intersecting the two lines was then measured, and an average fiber diameter and standard deviation were calculated using Image J software (National Institutes of Health).

3. Results & discussion

When the repulsive charges on the surface of the solution electrospinning jet create disturbance forces greater than the resisting viscoelastic forces in the jet, any bending instabilities in the jet become

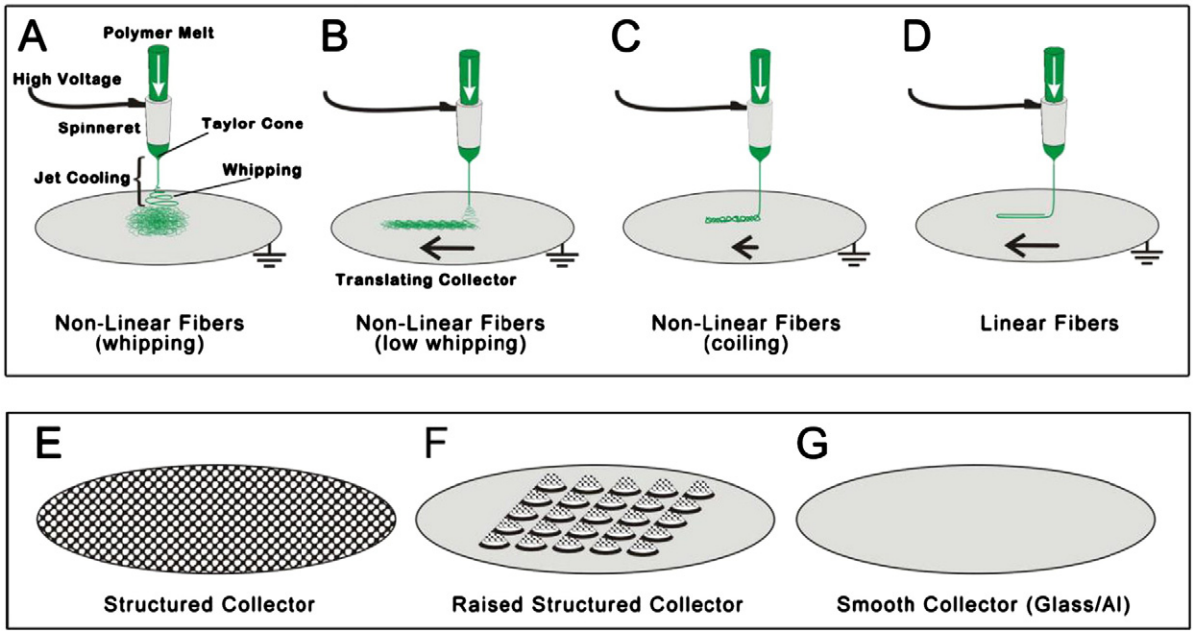

Fig. 1. Schematics of A) electrospinning subject to bending instabilities (often called whipping); B) melt electrospinning with diminished whipping, where the deposition of coiled fibers becomes focused on a translating collector; C) no whipping in the melt electrospinning jet. On a slow moving collector fibers are coiled, though focused; D) linear fibers result from increasing the collector speed to the critical translation speed; and various static fiber collection methods such as E) a stationary patterned electroconductive collector; F) array of patterned hemispherical collectors; and G) smooth collector surface (either Al or glass).

exaggerated in the presence of an electrical field, causing the jet to "whip" [31]. As the jet becomes unstable, the straight path of the stable jet turns erratic, causing fiber deposition to become highly random (Fig. 1A). Deposited fibers are coiled to create a nonwoven mat. If the surface charge density is decreased, the stable zone of the jet can be prolonged (Fig. 1B) [31,32]. Using high viscosity and non-conductive polymer melts instead of polymer solutions is one way to greatly reduce the surface charge density and therefore dampen any bending instabilities experienced by the melt jet [33]. Further, once the spinning temperature is below the glass transition temperature of the polymer, whipping of the jet is suppressed by fast solidification in the spinning region [5]. The initial stable region of the melt electrospinning jet is relatively much longer, resulting in a straight jet from the spinneret to the collector (Fig. 1C &D) [8]. As the melt jet impacts a stationary flat collector, it buckles under longitudinal compression, causing the fibers to coil around the initial point of impact (Fig. 1C). Such coiling patterns resemble those created by uncharged jets of highly viscous fluids impinging a hard flat surface [34]. The frequency of the coiling can be reduced by moving the collector [4], until a critical speed where the collected fiber is straight (Fig. 1D). In this processing state, the collector is moving faster than the molten electrified jet is being deposited, allowing fibers to be accurately placed.

3.1. Characterizing the influence of instrument parameters on fiber diameter

Similar to solution electrospinning, there are two important components to melt electrospinning fabrication: material- and instrument-based parameters. There are less material-based parameters than in solution electrospinning, where variables such as solvent type and solution concentration are not relevant. The most significant material-based parameter for melt electrospinning is the molecular weight of the polymer to be electrospun. With an increase in viscosity, resistance to melt flow through the spinneret becomes greater and limits the ability to extrude the polymer. Furthermore, the ability to electrostatically draw the emerging molten polymer jet is influenced by the viscosity; both morphologically and dimensionally. Once a suitable molecular weight polymer and operating temperature is established, the instrument-based parameters (e.g. electrospinning voltage, distance from the tip of the needle to collector, and flow rate) become important as they allow control over the resulting fiber diameter [26]. In addition, MEW requires further instrument parameter control; namely, the speeds and directions in which the collector is translated laterally to the path of the depositing melt jet strongly influence the accuracy of fiber placement [4].

When researchers are seeking to optimize processing parameters to obtain a continuous melt electrospun fiber with a specific morphology, the ability to gain immediate feedback on fiber morphology is beneficial. Although SEM allows highly detailed characterization and accurate measurement, it requires extensive sample preparation, can be time consuming, costly, and depends on instrument availability. Since SEM does not allow an immediate evaluation of the produced fibers, one widely used alternative is to electrospin directly onto a glass microscope slide and perform preliminary characterization using an OM. The glass slide can be introduced between the spinneret and the collector to collect fibers, removed without interrupting the process, and then placed immediately under an OM to provide the current status of an experiment. Such an approach allows *qualitative* assessment of fiber morphology, to confirm whether fibers are unbroken and have a consistent surface, so that instrument parameters can be adjusted in real time during an experiment towards optimal settings.

Since melt electrospinning is capable of producing fibers with diameters on the micron scale, *quantitative* analysis of fiber diameter via OM can also be readily performed. However, due to birefringence effects which occur when imaging fine fibers at high magnification, the accuracy of fiber diameter measurements using OM may be compromised. We compared fiber diameter measurements using images obtained from OM with SEM as represented in Fig. 2A. The graph in Fig. 2B demonstrates that using our particular microscopy configuration, measurements using OM agreed with SEM measurements for fiber diameters of 5 μm and above. Therefore, OM provides a convenient tool to accurately and steadfastly characterize melt electrospun fibers collected onto glass microscope slides.

To demonstrate the utility of OM characterization, glass microscope slides were used to collect fibers during an uninterrupted melt electrospinning experiment, where the effects of varying three key instrument parameters were measured. Fig. 2C demonstrates that the fiber diameter of melt electrospun PCL could be controlled from 5 μm to 35 μm. The combination of a low flow rate, low collection distance and high applied voltage appeared to result in the lowest diameter fibers, due to an enhanced electrostatic drawing force. In fact, at 5 μL/h flow rate, 10 mm collection distance and 12 kV applied voltage, the drawing force acted to pull the jet apart into broken fibers and as such a fiber diameter measurement is not recorded. Increasing the flow rate appears to have the most significant effect on increasing average fiber diameter, while decreasing the voltage could also be used to reduce the average fiber diameter. A greater material delivery rate reduces the density of the surface charge on the polymer and therefore diminishes the electrostatic drawing force. Above 5 μL/h flow rate, 4 kV applied voltage was insufficient to establish a Taylor cone. Increasing the collector distance appears to have a more significant effect on increasing the fiber diameter at higher polymer flow rates. At a flow rate of 20 μL/h, varying the voltage caused a wider range of fiber diameters when the collector distance was greater, where the electric field strength would be diminished according to a power law. At 20 μL/h flow rate and 10 mm collection distance, the electrostatic drawing force provided by 6 kV applied voltage was insufficient to sustain the Taylor cone and the melt electrospinning process ceased.

3.2. Melt electrospinning onto patterned electroconductive collectors

There are numerous studies in solution electrospinning which use modified collector substrates to create meshes which have large pores, while retaining sufficient mechanical integrity for handling/processing [1,14,15,17,18]. Usually metallic, these collectors can have repeating patterns of holes in them [15,17], or are stamped with a non-conductive substrate [18]. Adopting the former approach, the effect of melt electrospinning onto structured metallic collectors with varying repeating hole patterns was investigated in this study (Fig. 3A and D).

In solution electrospinning, the chaotic nature of the jet causes fibers to deposit randomly over a larger area on a smooth flat surface, compared to melt electrospinning where the jet is focused. A structured collector shows a degree of influence on fiber deposition for solution electrospun fibers, where fiber deposition is significantly more dense on the metallic surfaces [15,17]. However, the dynamic solution electrospinning jet causes many fibers to bridge the voids in the conductive collectors. In contrast, the melt electrospinning jet is less dynamic and initially fibers deposit exclusively onto the metallic regions of the collector. Previous studies support this observation, where collecting melt electrospun fibers across two metallic collectors separated by an air gap was shown to be limited to very short distances in the millimeter scale [8], while solution electrospun fibers were shown to bridge air gaps many centimeters in length [35].

The SEM images in Fig. 3 show scaffolds composed of relatively smooth and uniform continuous fibers with diameters in the range of 30–40 μm. Fig. 3B and E shows that the initial depositing fibers are attracted to the electroconductive material and preferentially align around the void geometries. Fig. 3B demonstrates how the majority of fibers have curved around the circular voids, with a dense accumulation of fibers around the edges of each pore. Similarly in Fig. 3E, the fibers

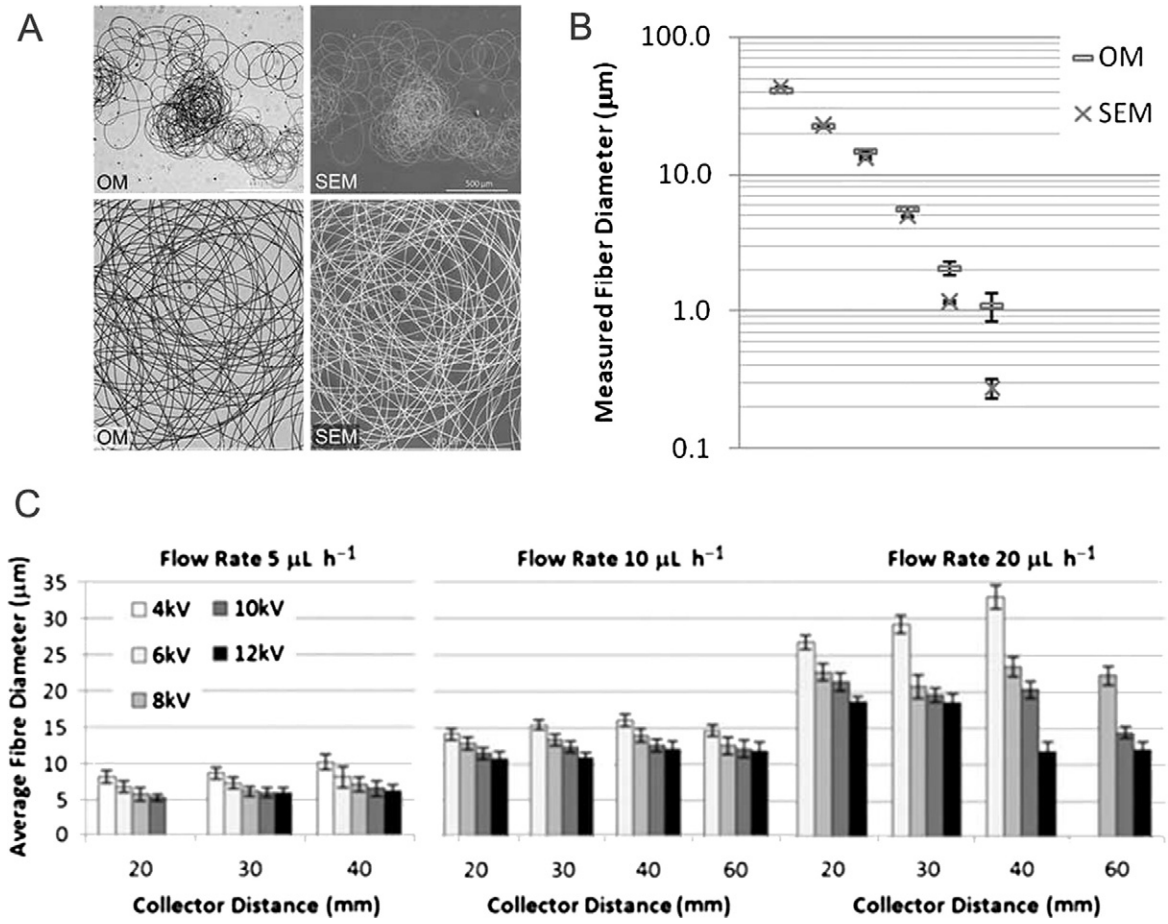

Fig. 2. Using OM to rapidly determine the effect of instrument parameters on the fiber diameter, where A) OM and SEM images taken at the same magnification and location on the sample are compared; B) fiber diameter measurements using each characterization method are compared. OM provides accurate quantification for fiber diameters above 5 µm compared to SEM; and C) OM measurements demonstrate the influence of varying melt electrospinning instrument parameters, flow rate, applied voltage and collector distance, on the collected fiber diameter.

conform to the shape of the electroconductive collector, where in this case straight fibers are aligned along the straight edges of the diamond-shaped voids.

As the scaffold thickness increases, the deposited fibers retain a small amount of electric charge which begins to insulate the melt electrospinning jet from the collector [34]. Fig. 3C shows the top surface of the scaffold following 30 min of collection, where the influence of the structured collector on fiber deposition has reduced and fibers have begun to cross over the air gaps. Again, in Fig. 3F there appears less control over the location of fiber deposition on the top surface as the scaffold thickness increases. Although there are regions of high fiber density which remain aligned according to the pattern of the collector, the fibers are closing in over the large pores. These experiments indicate that the distribution and alignment of melt electrospun fibers can be controlled using a patterned collector "template" to create scaffolds with shaped macroporous architectures with a limited thickness.

To investigate whether melt electrospinning onto multiple structured collectors during a single uninterrupted process would result in the previously described patterned fiber deposition effects, Fig. 4A shows an array of 20 wire mesh collectors upon a grounded moving plate. Each collector possessed a similar 400 µm × 400 µm square void template architecture. Rubber rings around the base of each filter provided a large separating air gap to reduce any disturbing influences on the jet's path from the adjacent collectors (Fig. 4B). The steel mesh of each earthed tap filter was dome shaped (Fig. 4C), where the highest point (shortest path for charge to be transported from the spinneret to ground) was located directly under the spinneret for the 20 min duration of fiber collection. This encouraged the melt jet to begin depositing in the center of the mesh and for fibers to be collected over a more uniform area. Fig. 4D demonstrates that the melt electrospun fibers arrange into dome shaped structures. Fig. 4E and F reveals the heterogeneous structure on the underside of the scaffold, where the open square shaped 400 µm pores match the architecture of the collector mesh. However, as demonstrated in Fig. 3, a closed fiber architecture developed on the top of the scaffold as the collection time increased and the average pore size reduced to 20 µm (Fig. 4D).

Following 20 min of fiber collection onto the first collector, the platform automatically moved to position the next collector centrally under the spinneret. A key observation from this study is that the melt electrospinning process was not interrupted: the jet would be dragged slightly in the direction of the departing collector, causing it to deform into a catenary profile, before tension in the melt jet would resist any further offset. The arrival of the new collector caused the jet to return to the center position (directly below the spinneret) and begin to deposit in the center of the next dome shaped collector. The absence of accumulated charge on the next collector resulted in ordered fiber collection until again a localized build-up of residual charge in the fibers would limit the control over fiber deposition. This process was repeated so that 20 similar scaffolds (Fig. 4B) could be fabricated automatically in a single batch. Importantly, this example demonstrates that a large number of melt electrospun samples can

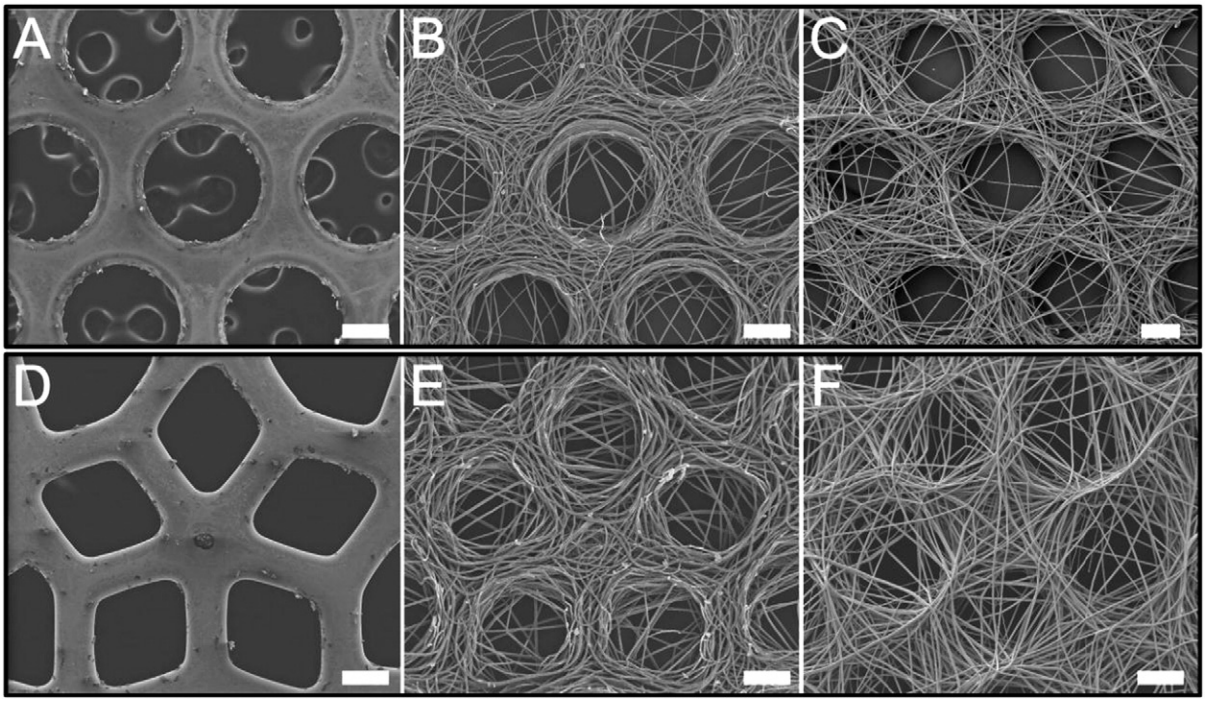

Fig. 3. Electroconductive collectors with different patterned voids A) & D) are shown to influence the location of melt electrospun fiber deposition; B) & E) show the underside of the corresponding scaffolds, where the fibers are first in contact with the collectors and assemble according to the shape of the electroconductive materials; C) & F) show the top of each patterned mesh, where shape fidelity is lost as the scaffold thickens and repulsive residual charge builds up through the fibrous layers. Scale bars 200 μm.

be effectively generated using an automated process. In total, 400 cell-invasive samples with repeatable architectures were fabricated in one week using this approach, for in vitro/vivo TE studies that are reported elsewhere [36].

3.3. Melt electrospinning onto stationary collectors

Following the observation that control of fiber deposition using structured collectors diminished over time, fiber collection characteristics

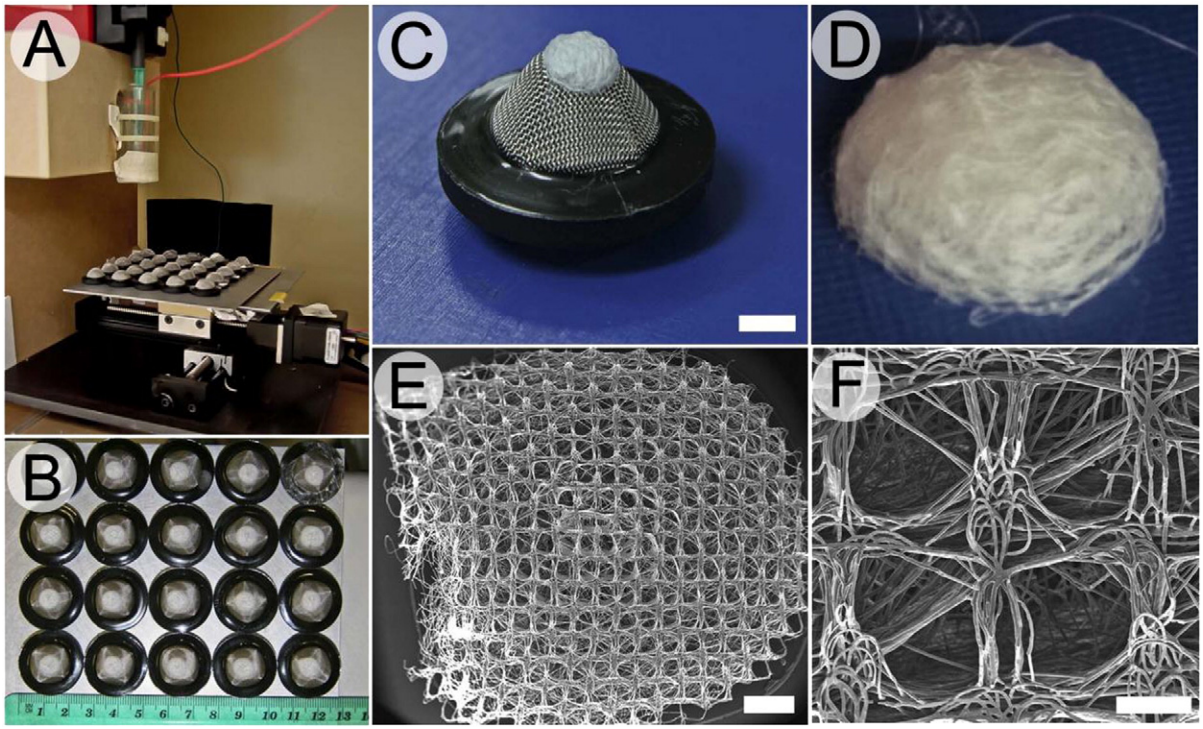

Fig. 4. Melt electrospinning onto A) an array of 20 patterned substrates with raised architectures. A moving collector is used to move each sample under the melt electrospinning jet; to create B) batches of replicable porous scaffolds from a biodegradable polymer; C) where the fibers deposit preferentially on the raised surface of the patterned collector; D) to create a domed structure similar to that of the collector; while E) retaining the square-shaped porous pattern of the collector on the underside of the scaffold; with F) an average pore size of 250 μm. Scale bars 5 mm, 1 mm and 200 μm for C), E) and F) respectively.

on static, flat surfaces were investigated. Typically metallic materials are used as collector substrates because their high electrical conductivity assists removal of charge from the depositing melt electrospun fibers [37–42]. However, collector substrate materials with different conductivities and surface charge characteristics could affect the collection behavior of fibers. Mitchell et al. reported that the dielectric strength and surface area of materials such as plastic could significantly distort the electric field and therefore affect the resulting fiber diameter and inter-fiber spacing [43]. Earlier it was demonstrated that glass microscope slides allow rapid characterization of melt electrospun fiber morphologies. This experiment investigated any differences in fiber deposition behavior between glass microscope slides and a metallic control, where glass microscope slides were wrapped in Al foil.

The slides were placed on a grounded platform, where computer-controlled movement allowed fibers to be automatically collected in discrete regions on the slides, for defined periods of deposition: pause times incremented from 1, 2, 5, 10, 20, 50 to 100 s (Fig. 5A). The graph in Fig. 5B indicates little effect between the surfaces on average fiber diameter for collection periods up to 100 s, though the fiber diameter is slightly lower for the first 2 s on the Al collector. This suggests that the use of glass microscope slides and OM is a valid approach for the expedient characterization of fiber morphologies, even when using a metallic collector which would not allow the fibers to be easily visualized under an OM.

Whereas in solution electrospinning fibers immediately deposit over a large surface area due to whipping effects [31], in melt electrospinning the fiber deposition is initially relatively focused. However, the deposited fibers retain a small amount of residual Coulombic charge and begin to insulate the melt jet from the conducting collector as the stored charge builds up. Over time, newly depositing fibers are repelled outwards from the initial collection point, where the surrounding uncovered collection surface provides less resistance for charge to be transported to ground [34]. The result is a growing circular mesh of coiled fibers with a relatively uniform thickness [44]. The table in Fig. 5C shows that for collection times of 50 s or less, there were no statistically significant differences between the average areas of the circular meshes using glass or Al collectors. However, for collection times above 50 s, there was a slight increase in the mean mesh area for the microscope slides compared to the Al foil, where the glass material would be less efficient at transporting charge to ground.

Fig. 5 also shows the growth of the circular meshes from Fig. 5A over increasing durations. The initial random nature of fiber coiling is similar on both Al and glass microscope slide surfaces after 10 s, where fiber deposition is governed by the wavelength of buckling (approximately 500 μm in this case). As the polymer fibers increase in density, the jet is repelled from the like charged fibers and attracted to the unexposed part of the collector. This causes the point of contact between the jet and the collector to move outwards over a larger surface area. However, the resulting deviation of the jet profile from the midline (Fig. 6A) due to electrostatic forces is resisted by viscoelastic tensile stresses in the melt jet [34]. After 20 s of collection in Fig. 5, a point is reached where the increasing tension in the melt jet begins to resist any further travel away from the midline, and a maximum collection area is reached.

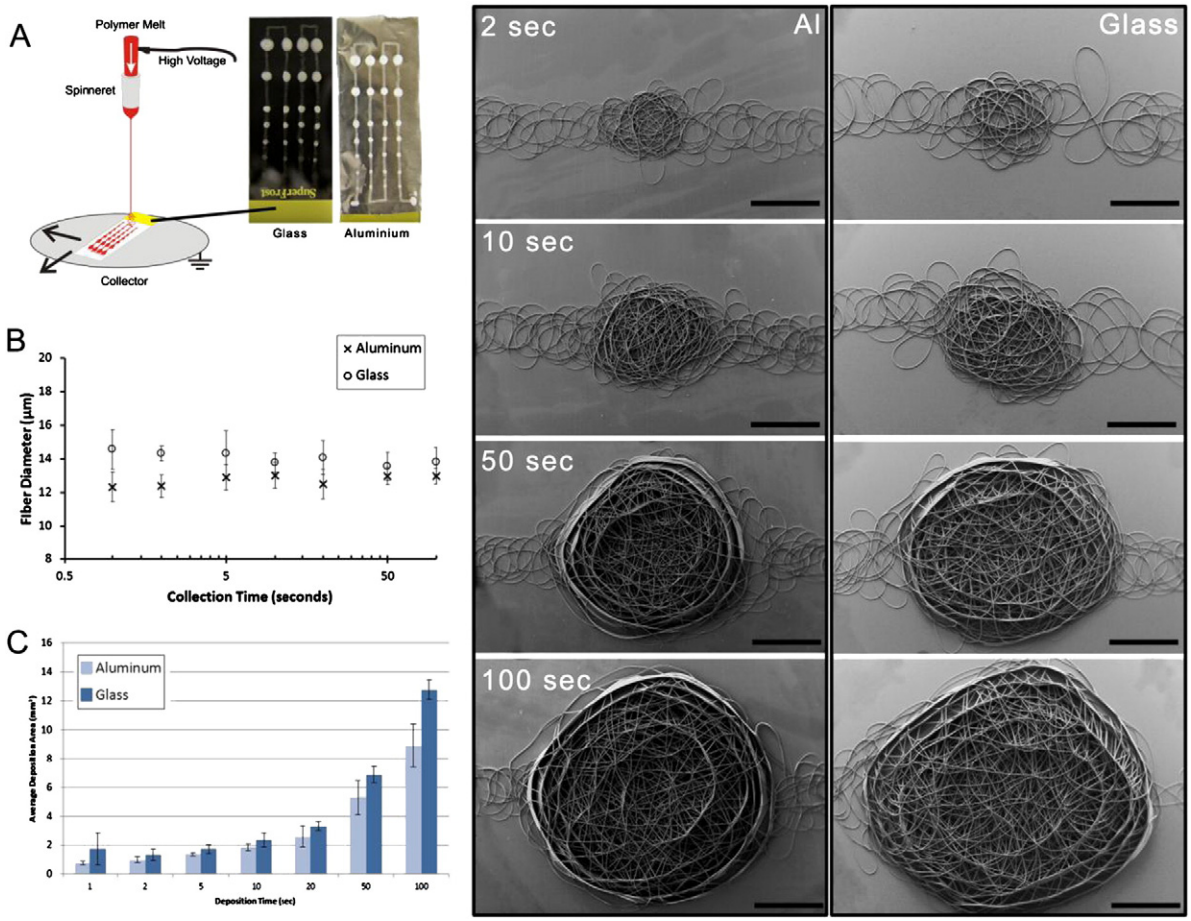

Fig. 5. A) A schematic showing melt electrospinning for increasing durations onto stationary glass and Al covered microscope slides. A single microscope slide was placed on a grounded x–y stage collector which was programmed to pause for incremental collection times from 1 s to 100 s; B) the measured fiber diameters for each collection period on both substrates are compared; as well as C) the measured areas over which fibers deposit for each collection time. On the right are SEM images of melt electrospun fibers collected onto stationary Al foil covered (left) or glass microscope slides (right), with increasing collection times. Scale bars 1 mm.

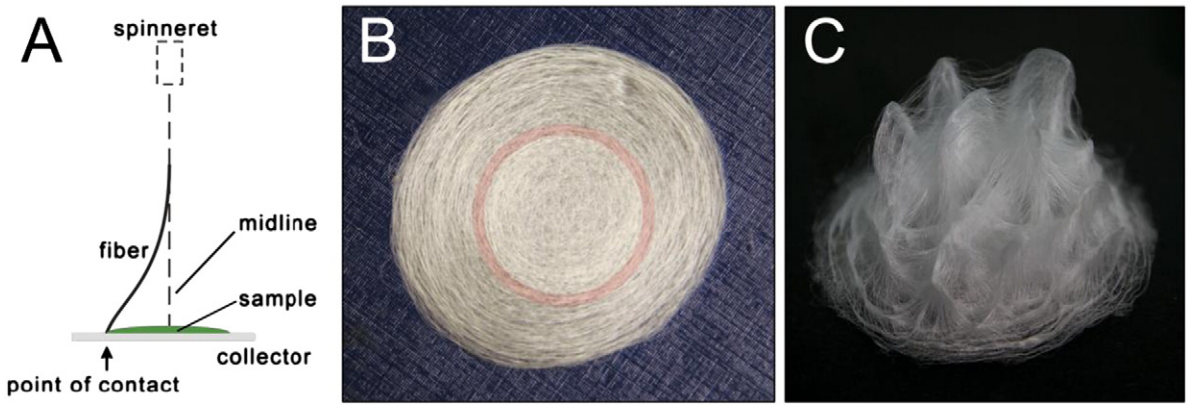

Fig. 6. A) Schematic showing deflection of the melt electrospinning jet profile away from the midline due to the buildup of repulsive electric charge in the collected fibers (stationary collector); B) initially the fibers deposit randomly and are coiled due to buckling (inside highlighted pink circle) until tension develops in the jet, which resists further deflection of the jet profile. The repulsive charges in the mesh cause the jet to adopt a pendulum motion where the jet circles the perimeter of the mesh (outside the highlighted pink circle); until C) the fibers begin to stack on top of each other towards the spinneret to create a conical 3D structure.

The tensile forces induced in the melt electrospinning jet dampen the compressive buckling forces, causing the frequency of coiling to decrease and the wavelength of coiling to increase [34]. This is seen around the edges of the meshes in Fig. 5, where after 50 s the fibers begin to coil in a pendulum motion around the perimeter of the mesh, to create a circular ribbon-like structure of fused fibers stacked on top of each other.

After 100 s collection time in Fig. 5, the tension in the melt jet causes the ribbon-like stack of fibers to spiral towards the center of the circular mesh. With the build-up of repulsive charge in the mesh, the melt electrospinning jet reduces in length to maintain sufficient electrostatic driving potential, seeking the highest point in the fibrous construct [9]. The fibers stack on top of each other to create a conical structure, growing upwards towards the spinneret. Such a fiber deposition phenomenon is not typically observed in solution electrospinning onto smooth, flat surfaces due to several factors: the fibers are spread over a larger surface area due to whipping of the jet; and the enhanced buildup in electric charge on the relatively flat mesh of deposited fibers sees the solution jet repelled away from the collector before 3D constructs can be fabricated.

When all of the other melt electrospinning parameters were held constant, increasing the spinneret to collector distance from 20 mm (Fig. 5) to 50 mm (Fig. 6B) was demonstrated to increase the fiber deposition area. An increased jet length increases the natural wavelength of the jet, as well as reducing the electric field strength in the experiment, which decreases the jet velocity at impact with the collector. These two factors combine to increase the wavelength of fiber coiling, where inside the highlighted pink region in Fig. 6B the randomly deposited fibers are less densely packed than in Fig. 5. Outside of the highlighted region in Fig. 6B, the increase in coiling wavelength is visible without microscopy, where the fibers begin to loop in a circular manner around the perimeter of the mesh. With a reduced electrostatic driving force, the fibers are less densely packed before the onset of fiber stacking, where after several hours the tensile limit in the jet is reached and the fibers begin to stack vertically to create conical structures such as that shown in Fig. 6C.

3.4. Melt electrospinning writing

The previous section demonstrated that on a flat stationary collector surface the melt jet will eventually reach a maximum area of fiber deposition, where the tensile stresses developed in the jet resist further deflection of the jet profile away from the midline due to the repulsive stored charge in the collected fibers. Instead, the stored repulsive charge in the fibers forces the jet to adopt a pendulum motion around the perimeter of the fibrous mesh [34]. Another approach to induce tension in the melt electrospinning jet is to introduce relative motion between the collector and the spinneret. If the collector is moved laterally to the path of the jet, a tensile drag force between the collector and the depositing jet will act to resist deformation of the jet profile from the

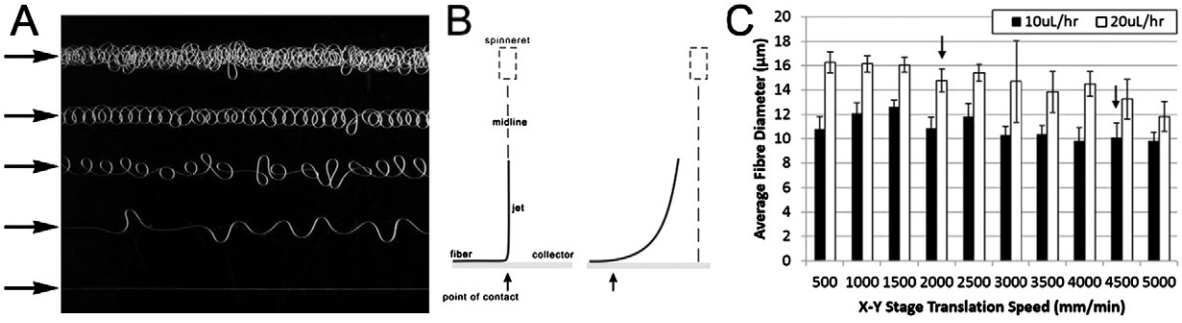

Fig. 7. A) Melt electrospun fibers collected onto a grounded flat collector, programmed to translate in straight lines (in the direction of the arrows) with increasing speed (from top to bottom). Initially the fibers are coiled due to buckling, then the wavelength of the coiling decreases with increasing collector speed. When the collector speed matches the melt electrospinning jet speed (critical translation speed), the wavelength of fiber coiling becomes infinite and a straight fiber in the direction of collector movement results (bottom); B) at the critical translation speed, compressive buckling forces are matched by tensile forces in the jet (created by drag between the jet and the collector surface). The jet profile is straight (left) and impacts the collector directly below the spinneret. If the collector is moved above the critical translation speed, tensile drag forces increase, causing the jet profile to deform and the point of impact to lag behind the midline; C) faster translation speeds cause a slight reduction in average fiber diameter. Arrows show that the critical translation speed varies for different fiber diameters (where the jet speed will decrease for larger fiber diameters).

straight (shortest) path to ground. Similar to the situation previously described, such a tensile force will act against the compressive buckling phenomenon to reduce the wavelength of fiber coiling [4].

If the collector is translated in a straight line with an increasing speed (from top to bottom in Fig. 7A), the tensile drag force in the melt electrospinning jet increases accordingly, acting to reduce the wavelength of fiber coiling. As is described schematically in Fig. 1C to D, there is a critical point where the collector speed equals the speed of the melt electrospinning jet, at which the compressive buckling and tensile drag forces balance and the wavelength of depositing fiber coiling becomes infinite [4]. At this point, fiber deposition occurs directly below the spinneret, as shown on the left in Fig. 7B, and a straight fibrous line in the direction of collector movement results (bottom of Fig. 7A).

If the collector is moved at greater speeds, the tensile drag force increases above the compressive buckling force, causing several effects: the jet profile deforms away from the midline and the impact point begins to "lag" behind (Fig. 7B right); while Fig. 7C demonstrates that a degree of mechanical drawing is imparted on the collected fibers, reducing the average fiber diameter. However, the reduction in average fiber diameter due to increased collector speed (Fig. 7C) is modest compared to changing an instrument parameter such as flow rate of the polymer melt to the spinneret (Fig. 2). An observed effect is that increasing the flow rate acts to slow the speed of the melt electrospinning jet [4]. The consequence of this is shown in Fig. 7C, where the critical speed to achieve a straight melt electrospun fiber is lower when a higher flow rate is used. Since the flow rate is proportional to the average fiber diameter, this produces a general rule that *at the critical translation speed* the smaller diameter fibers require a faster translation speed to remove coiling and write straight fibrous lines [4].

If an automated collector is programmed to translate continuously at the critical speed in different directions, a process termed MEW occurs, allowing scaffolds consisting of fibrous lines to be constructed with complex patterns (Fig. 8A). Such an approach can produce two classes of fibers – coiled and linear – where the transition from random nonwoven fibers to accurate placement is primarily dependent on the collector translation speed. While the mechanical effect of operating above the critical translation speed does begin to reduce the fiber diameter, it is at the expense of placement accuracy. For controlling changes in fiber diameter, it is more effective to alter the flow rate and operate just above the relevant critical translation speed.

3.5. Limits of substrate height and accurate fiber placement

The production of true 3D objects using electrospinning relies on the ability to stack fibers one upon another and have them fuse together to create a coherent structure. Since electrostatic forces are used to draw the electrospinning jet into fibers, both shielding and residual charges upon the deposited fibers can affect deposition accuracy, as previously shown in Figs. 5 and 6 when collecting onto a stationary collector. This effect is also commonly observed in solution electrospinning, where deposited fibers repel the newly depositing fibers, producing challenges in the formation of 3D structures. However many of the residual charges in that instance are contributed by the remaining solvent that has not fully evaporated. Since melt electrospinning is solvent free, it would be expected that a greater volume of fibers could be deposited, to more readily form a 3D structure.

Indeed melt electrospinning can produce structures with significant height – many cm – as shown in Fig. 6C. However, for 3D printing applications it is important to achieve structures *with accurate fiber placement*. Fig. 8B demonstrates that the 20 μm average diameter linear fibers which create the pattern fabricated in Fig. 8A using MEW, can be continuously and accurately placed on top of each other to create an ordered structure—consisting of an array of 1 mm × 1 mm boxes. The automated moving collector repeatedly translated the path, which defines the pattern in Fig. 8A, to create a structure with a height of approximately 1 mm. Fig. 8C demonstrates that 50 layers of the repeating box pattern could be placed on top of each other before electrostatic repulsion from residual charge on the fibers induced a significant loss of placement resolution.

3.6. Fiber placement accuracy during writing

Considering the repeatability of the moving x–y stage used (±50 μm), it may be considered surprising that for each of the first 50 layers of deposition, the fibers in Fig. 8 deposit directly on top of each other. This suggests that in this case the jet is in fact *attracted* to, rather than repulsed by, the previously deposited filament. We suggest an explanation for this phenomenon: although the fiber may contain a degree of residual charge which would be expected to repel the jet, this charge may be trapped in the internal structure of the fiber. Furthermore, the difference between this stored charge potential in a single fiber and the grounded collector may be so low that the physical geometry of the fiber plays a greater influence on the path of charge transport. In cross section, the fiber would appear as a point raised above the flat grounded surface and therefore offer a shorter path for the jet to discharge to a lower potential surface. The majority of charge would be transported to ground across the surface of the fiber, while the residual charge is trapped inside the fiber as it completely solidifies. As the fibers continue to stack up to a significant height (50 layers) as seen in Fig. 8C, the amount of collective charge stored in the fibers becomes sufficient to begin to repel the jet and exact fiber placement is lost.

While the distance between parallel 20 μm diameter fibers in Fig. 8 was relatively large (1 mm), Fig. 9A demonstrates the result of programming a step-wave pattern where the spacing between parallel lines is reduced to 10 μm. At the edges of the construct there are coiled fibers, where the program included a brief pause after each turn, so that before each (horizontal) straight line segment was written there was minimal mechanical influence on the path of the jet due to tensile drag. In this

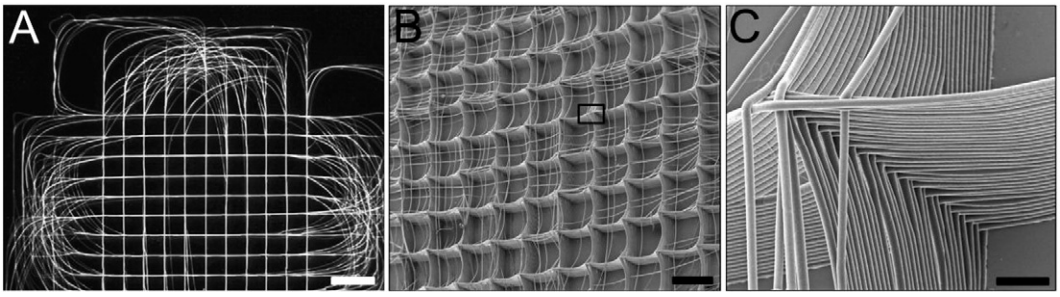

Fig. 8. A) Melt electrospun fibers are collected onto a grounded flat collector programmed to translate continuously at the critical speed in different straight line directions; B) this process, MEW, allows 3D structures consisting of straight fibrous lines to be constructed with repeating patterns. Fibers can be accurately placed on top of each other many times; before C) a build-up of repulsive charge in the fibers causes the jet to deflect, and the accuracy of fiber placement is lost. The scale bars are 2 mm, 1 mm and 100 μm in A), B) and C) respectively.

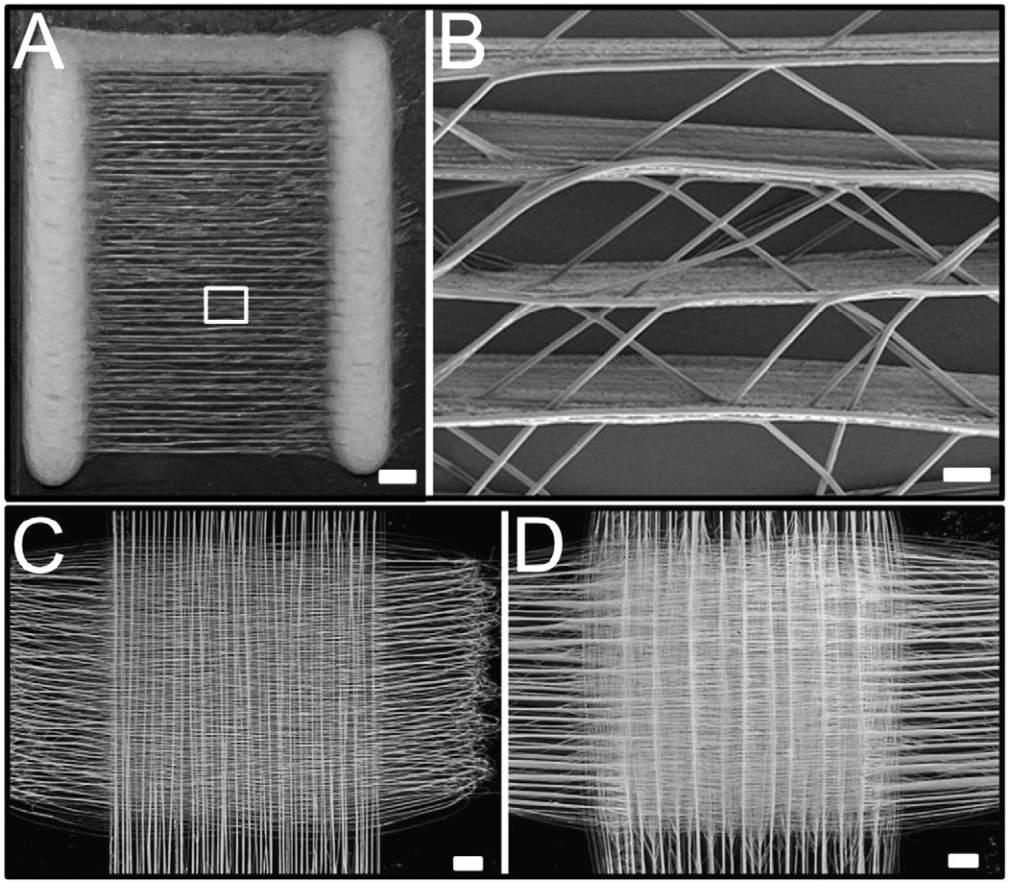

Fig. 9. A) MEW of a step-wave pattern. Coiled fibers at the edges of the construct are the result of a brief pause in the program after each turn; B) top view of ribbons of parallel fiber stacks spaced at approximately 300 μm. After approximately 20 layers, fiber placement is disturbed by accumulated charge in the fibers, as seen by fibers crossing over between adjacent stacks; C) underside of scaffold fabricated from fibers collected with straight lines written above the critical translation speed. The fibers lag behind the programmed step (square) pattern in the turning regions and "cut the corner" as loops, however, the extra tension in the melt jet provides greater resistance to the disturbing electric forces and allows fibers to be placed in closer proximity; D) as fiber collection continues over several hours, the buildup of residual charge in the scaffold causes the electric forces to dominate the tensile mechanical forces and the fiber stacks begin to fan away from each other (top view). The scale bars are A) 1 mm, B) 100 μm, and C&D) 1 mm.

case adjacent horizontal fibers (which were written at the critical translation speed) were observed to stack on top of each other in a similar manner to Figs. 5 and 8. Fig. 9B shows ribbons of fiber stacks spaced at approximately 300 μm, rather than fibers placed down beside each other with the programmed 10 μm spacing. After approximately 20 layers in Fig. 9B, the fiber placement begins to become disturbed. The fibers are observed to be deflected from their straight path and begin to cross over to adjacent fiber stacks. This could be attributed to slight height differences between the fiber stacks as they form, or differences in the cumulative charge in each stack, where the jet seeks the path of least resistance to discharge to ground.

Fig. 9C illustrates an approach investigated to reduce the distance between deposited parallel fibers, by attempting to resist the electrical disturbing forces in Fig. 9B with mechanical forces. Here, the collector speed was increased above the critical translation speed to increase the tensile drag force acting on the jet. One compromise to this approach is observed on the right in Fig. 9C, where the looped fibers lag behind the programmed step (square) pattern in the turning regions and "cut the corner" [4]. However, increasing the tension in the melt electrospinning jet reduced the average distance between parallel fiber stacks from 300 μm (Fig. 9B) to 200 μm in the layers close to the grounded collector (Fig. 9C). From the diameter of the looped fibers in Fig. 9C, it would appear that the viscoelasticity of the jet may become a limiting factor on how tightly the jet can turn when using such a square wave writing approach. As fiber collection in Fig. 9C continued over several hours, the typically observed buildup of residual charge in the scaffold caused the fiber stacks to fan away from each other. The top view of the scaffold in Fig. 9D shows that the fiber stacks have become separated by approximately 1 mm.

4. Conclusions

Even though melt electrospinning is increasingly described in the literature, there remains a general lack of melt electrospinning expertise, in particular to build large volume scaffolds with reproducible features for use in the biomaterial and TE fields. One key factor is the absence of knowledge regarding charge transport in melt electrospun fibers, which limits the predictability of fiber placement over time due to charge interactions between collected fibers. Various melt electrospinning fiber collection approaches were investigated in this study to fabricate scaffolds with interconnected pores large enough to be cell invasive and suitable for vascularization. We also demonstrated a method which allows rapid fiber characterization, to assess the influence of varying in process operating parameters on fiber morphology, without the need to interrupt a melt electrospinning experiment. OM provides accurate quantification for fiber diameters above 5 μm compared to SEM.

When the focused melt electrospinning jet impacted a stationary flat collector, the following characteristics of fiber deposition were observed: initially, compressive buckling caused the solidifying fibers to randomly coil around the point of impact directly below the spinneret. This phenomenon is different to solution electrospinning, where whipping of the electrified jet distributes the coiled fibers over a significantly larger area at the onset of deposition [31,32,45]. Over time, the buildup

of residual charge in the collected melt electrospun fibers caused the jet profile to deflect outwards from the midline and the area of the circular nonwoven mesh of fibers increased. Tensile stresses developed in the melt electrospinning jet to resist further outward deformation of the jet profile and instead the jet was deflected around the perimeter of the circular mesh by the repulsive charges, following a pendulum motion. Eventually the fibers stacked vertically to create a conical structure which grew towards the spinneret. Similar fiber deposition phenomena were observed on metallic and glass substrates.

Electroconductive collectors with different patterned voids were shown to influence the location of melt electrospun fiber deposition. The charged melt electrospinning jet deflected towards and deposited preferentially onto the conducting substrates, where the fibers aligned according to the patterned surfaces. Shape fidelity was lost as the scaffold thickened, where repulsive residual charge built up through the fibrous layers. Batches of replicable porous scaffolds showed this effect is reproducible to fabricate architecturally ordered scaffolds.

MEW was demonstrated as a additive manufacturing approach to produce ordered TE scaffolds with enhanced control over fiber placement. MEW offers improved filament resolutions over processes such as FDM for the processing of polymer melts. In melt extrusion based direct writing, where the polymer is applied from the nozzle directly onto a collector substrate, the filament placement resolution is largely controlled by the precision of the moving parts of the machine. MEW on the other hand, involves the added complexities of controlling coiling of the melt jet and disturbing electric charge interactions. Translating a flat collector surface laterally to the melt electrospinning jet introduced a tensile drag force between the collector and the jet. The tensile force increased as the collector was translated faster, causing the wavelength of compressive buckling at the impact point on the collector to increase. When the collector translated at the critical translation speed in a straight line, coiling did not occur. Instead the fiber deposited directly below the spinneret as a continuous straight line in the direction of collector movement. Faster collector speeds deformed the jet profile away from the midline, causing a loss of accuracy in fiber placement due to lag.

These observations of fiber deposition demonstrate that translating the collector according to a pre-programmed pattern at the same speed as the melt electrospinning jet allowed the writing of coherent 3D fibrous structures with well controlled porous architectures. The height that a melt electrospun scaffold could be accurately fabricated was influenced by the pattern deposited (including the spacing between fibers), the speed of translation, as well as the buildup of residual charge in the fibers. Further understanding of how the viscous, electrically charged melt electrospinning jet interacts with the collector surface will improve the accuracy and repeatability of fiber deposition, towards developing this process as a 3D printing approach. We are confident that these insights will facilitate improved design and fabrication of ordered MEW structures for application in TE.

Acknowledgments

Technical assistance from Dr. Christina Theodoropoulos, Dr. Derrick Maxwell and Mr. Wolfgang Maier is greatly appreciated.

References

[1] D.W. Hutmacher, T. Woodfield, P.D. Dalton, J. Lewis, Scaffold design and fabrication, in: C. Van Blitterswijk, P. Thompsen, A. Lindhal, J. Hubbell, D.F. Williams, R. Cancedda, J.D. de Bruijn, J. Sohier (Eds.), Tissue Engineering, Academic Press, 2008, pp. 403–450.
[2] P.D. Dalton, T. Woodfield, D.W. Hutmacher, Biomaterials 30 (12) (2009) 2420-2420.
[3] P.D. Dalton, C. Vaquette, B.L. Farrugia, T.R. Dargaville, T.D. Brown, D.W. Hutmacher, Biomater. Sci. 1 (2) (2013) 171–185.
[4] T.D. Brown, P.D. Dalton, D.W. Hutmacher, Adv. Mater. 23 (47) (2011) 5651–5657.
[5] D.W. Hutmacher, P.D. Dalton, Chem. Asian. J. 6 (1) (2011) 44–56.
[6] G. Srinivasan, D.H. Reneker, Polym. Int. 36 (2) (1995) 195–201.
[7] T. Subbiah, G.S. Bhat, R.W. Tock, S. Pararneswaran, S.S. Ramkumar, J. Appl. Polym. Sci. 96 (2) (2005) 557–569.
[8] P.D. Dalton, D. Grafahrend, K. Klinkhammer, D. Klee, M. Moller, Polymer 48 (23) (2007) 6823–6833.
[9] C. Mota, D.D. Puppi, M.M. Gazzarri, P.P. Bártolo, F. Chiellini, Polym, Int 62 (6) (2013) 893–900.
[10] V. Karageorgiou, D. Kaplan, Biomaterials 26 (27) (2005) 5474–5491.
[11] R.L. Dahlin, F.K. Kasper, A.G. Mikos, Tissue Eng. B Rev. 17 (5) (2011) 349–364.
[12] N. Bhardwaj, S.C. Kundu, Biotechnol. Adv. 28 (3) (2010) 325–347.
[13] M. Simonet, O.D. Schneider, P. Neuenschwander, W.J. Stark, Polym. Eng. Sci. 47 (12) (2007) 2020–2026.
[14] W. Cui, J. Chang, P.D. Dalton, Electrospun fibers for drug delivery, in: P. Ducheyne (Ed.), Comprehensive Biomaterials, vol. 4, Elsevier, 2011, pp. 445–462.
[15] D. Zhang, J. Chang, Adv. Mater. 19 (21) (2007) 3664–3667.
[16] J. Rnjak-Kovacina, A.S. Weiss, Tissue Eng. B Rev. 17 (5) (2011) 365–372.
[17] C. Vaquette, J.J. Cooper-White, Acta Biomater. 7 (6) (2011) 2544–2557.
[18] A. Karchin, Y.N. Wang, J. Sanders, J. Biomed. Mater. Res. A 100 (6) (2012) 1605–1614.
[19] S. Agarwal, A. Greiner, Polym. Adv. Technol. 22 (3) (2011) 372–378.
[20] H.C. Chen, W.C. Jao, M.C. Yang, Polym. Adv. Technol. 20 (2) (2009) 98–103.
[21] B.L. Farrugia, T.D. Brown, Z. Upton, D.W. Hutmacher, P.D. Dalton, T.R. Dargaville, Biofabrication 5 (2) (2013) 025001.
[22] C. Vaquette, S. Ivanovski, S.M. Hamlet, D.W. Hutmacher, Biomaterials 34 (22) (2013) 5538–5551.
[23] L. Thibaudeau, A. Taubenberger, B.M. Holzapfel, V.M. Quent, T. Fuehrmann, P. Hesami, T.D. Brown, P.D. Dalton, C.A. Power, B. Hollier, D.W. Hutmacher, Dis. Mod. Mech. 7 (2) (2014) 299–309.
[24] H.J. Zhou, T.B. Green, Y.L. Joo, Polymer 47 (21) (2006) 7497–7505.
[25] P.D. Dalton, N.T. Joergensen, J. Groll, M. Moeller, Biomed. Mater. 3 (3) (2008).
[26] T.D. Brown, A. Slotosch, L. Thibaudeau, A. Taubenberger, D. Loessner, C. Vaquette, P.D. Dalton, D.W. Hutmacher, Biointerphases 7 (1–4) (2012) 13.
[27] M. Gazzarri, C. Bartoli, C. Mota, D. Puppi, D. Dinucci, S. Volpi, F. Chiellini, J. Bioact. Compat. Polym. 28 (5) (2013) 492–507.
[28] C. Wei, J. Dong, J. Micromech. Microeng. 23 (2) (2013) 025017.
[29] J. Ko, N.K. Mohtaram, F. Ahmed, A. Montgomery, M. Carlson, P.C. Lee, S.M. Willerth, M.B. Jun, J. Biomater. Sci. Polym. Ed. 25 (1) (2014) 1–17.
[30] A. Cipitria, A. Skelton, T.R. Dargaville, P.D. Dalton, D.W. Hutmacher, J. Mater. Chem. 21 (26) (2011) 9419–9453.
[31] A. Yarin, S. Koombhongse, D. Reneker, J. Appl. Phys. 89 (2001) 3018.
[32] A. Yarin, S. Koombhongse, D. Reneker, J. Appl. Phys. 90 (9) (2001) 4836–4846.
[33] E. Zhmayev, H. Zhou, Y.L. Joo, J. Non-Newtonian Fluid Mech. 153 (2–3) (2008) 95–108.
[34] T. Han, D.H. Reneker, A.L. Yarin, Polymer 49 (8) (2008) 2160–2169.
[35] P.D. Dalton, D. Klee, M. Moller, Polymer 46 (3) (2005) 611–614.
[36] D.W. Hutmacher, S. Zaiss, A. Berner, M. Kim, A. Taubenberger, T.D. Brown, In vitro Study of Ovine Mesenchymal Progenitor Cells, Osteoblasts Isolated from Long Bone and Orofacial Bone on Melt Electrospun Scaffolds 9th World Biomaterials Congress Chengdu, China, 2012.
[37] X.-f. Wang, Chin. J. Polym. Sci. 28 (1) (2010) 45–53.
[38] Z.K. Nagy, A. Balogh, G. Drávavölgyi, J. Ferguson, H. Pataki, B. Vajna, G. Marosi, J. Pharm. Sci. 102 (2) (2013) 508–517.
[39] R. Nayak, I.L. Kyratzis, Y.B. Truong, R. Padhye, L. Arnold, J. Mater. Sci. 47 (17) (2012) 6387–6396.
[40] R. Nayak, R. Padhye, I.L. Kyratzis, Y.B. Truong, L. Arnold, Text. Res. J. 83 (6) (2013) 606–617.
[41] J. Ko, N.K. Mohtaram, F. Ahmed, A. Montgomery, M. Carlson, P.C. Lee, S.M. Willerth, M.B. Jun, J. Biomater. Sci. Polym. Ed. (2013) 1–17 (ahead-of-print).
[42] P.D. Dalton, J. Lleixà Calvet, A. Mourran, D. Klee, M. Möller, Biotechnol. J. 1 (9) (2006) 998–1006.
[43] S. Mitchell, J. Sanders, J. Biomed. Mater. Res. A 78 (1) (2006) 110–120.
[44] P. Heikkilä, L. Söderlund, J. Uusimäki, L. Kettunen, A. Harlin, Polym. Eng. Sci. 47 (12) (2007) 2065–2074.
[45] A. Yarin, W. Kataphinan, D. Reneker, J. Appl. Phys. 98 (6) (2005) (064501-064501-064512).